Langmuir
Article
pubs.acs.org/Langmuir

Wrinkled, Dual-Scale Structures of Diamond-Like Carbon (DLC) for Superhydrophobicity

Yudi Rahmawan,[†,‡] Myoung-Woon Moon,*[,‡] Kyung-Suk Kim,[§] Kwang-Ryeol Lee,[‡] and Kahp-Yang Suh*[,†]

[†]*School of Mechanical and Aerospace Engineering, WCU program for Multiscale Design, Seoul National University, Seoul 151-742, Republic of Korea,* [‡]*Convergence Technology Laboratory, Korea Institute of Science and Technology. Seoul 130-650, Republic of Korea, and* [§]*Division of Engineering, Brown University, Providence, Rhode Island 02912*

Received June 13, 2009. Revised Manuscript Received September 15, 2009

We present a simple two-step method to fabricate dual-scale superhydrophobic surfaces by using replica molding of poly(dimethylsiloxane) (PDMS) micropillars, followed by deposition of a thin, hard coating layer of a SiO_x-incorporated diamond-like carbon (DLC). The resulting surface consists of microscale PDMS pillars covered by nanoscale wrinkles that are induced by residual compressive stress of the DLC coating and a difference in elastic moduli between DLC and PDMS without any external stretching or thermal contraction on the PDMS substrate. We show that the surface exhibits superhydrophobic properties with a static contact angle over 160° for micropillar spacing ratios (interpillar gap divided by diameter) less than 4. A transition of the wetting angle to approximately 130° occurs for larger spacing ratios, changing the wetting from a Cassie−Cassie state (C^m-C^n) to a Wenzel−Cassie state (W^m-C^n), where m and n denote micro- and nanoscale roughness, respectively. The robust superhydrophobicity of the Cassie−Cassie state is attributed to stability of the Cassie state on the nanoscale wrinkle structures of the hydrophobic DLC coating, which is further explained by a simple mathematical theory on wetting states with decoupling of nano- and microscale roughness in dual scale structures.

Introduction

Surface modification in the form of either chemical treatment or texturing has been developed for functionalizing surfaces with potential applications for biological arrays,[1,2] microfluidics,[3] biomedical devices,[4,5] and smart reversible/anisotropic wetting surfaces.[6−8] In particular, there has been extensive effort to achieve water-repelling surfaces decorated with hierarchical structures similar to those found on a lotus leaf.[9] Simple theoretical models have also been developed to describe the geometrical and chemical contributions of the surface structures to wetting behaviors of a water droplet on many different solid surfaces.[6,10−13]

In general, superhydrophobic surfaces can be prepared by dual-scale hierarchical roughness surface structures made of low-surface-energy materials. One can sculpt bulk materials into smaller surface structures by photolithography,[14,15] soft lithography,[16,17] and plasma treatment,[12,18,19] or alternatively build or integrate small parts into larger structures by self-assembly or self-organization processes such as chemical synthesis,[20,21] thin film deposition,[22] or wrinkled patterns by plasma treatment.[23]

Here, we present an alternative method of creating three-dimensional (3-D) dual-scale superhydrophobic surface structures by depositing a thin layer of diamond-like carbon (DLC) coating with high compressive stress on a prepatterned poly(dimethylsiloxane) (PDMS, $(C_2H_6OSi)_n$) substrate. Using the well-known method of PDMS replica molding, a micropillar array can be fabricated with different spacing ratios to explore the effect of microscale roughness on hydrophobicity (Figure 1a,b). Then, we cover the micropillar array with a nanoscale wrinkle pattern by depositing a thin compressed SiO_x-incorporated DLC

*Corresponding authors E-mail: sky4u@snu.ac.kr or mwmoon@kist.re.kr.

(1) Chen, C. S.; Mrksich, M.; Huang, S.; Whitesides, G. M.; Ingber, D. E. *Science* **1997**, *276*, 1425–1428.
(2) Wang, Y. L.; Sims, C. E.; Marc, P.; Bachman, M.; Li, G. P.; Allbritton, N. L. *Langmuir* **2006**, *22*, 8257–8262.
(3) Gau, H.; Herminghaus, S.; Lenz, P.; Lipowsky, R. *Science* **1999**, *283*, 46–49.
(4) Xu, L. B.; Chen, W.; Mulchandani, A.; Yan, Y. S. *Angew. Chem., Int. Ed.* **2005**, *44*, 6009–6012.
(5) Tao, S. L.; Popat, K. C.; Norman, J. J.; Desai, T. A. *Langmuir* **2008**, *24*, 2631–2636.
(6) Caputo, G.; Cortese, B.; Nobile, C.; Salerno, M.; Cingolani, R.; Gigli, G.; Cozzoli, P. D.; Athanassiou, A. *Adv. Funct. Mater.* **2009**, *19*, 1149–1157.
(7) Athanassiou, A.; Lygeraki, M. I.; Pisignano, D.; Lakiotaki, K.; Varda, M.; Mele, E.; Fotakis, C.; Cingolani, R.; Anastasiadis, S. H. *Langmuir* **2006**, *22*, 2329–2333.
(8) Xia, F.; Feng, L.; Wang, S. T.; Sun, T. L.; Song, W. L.; Jiang, W. H.; Jiang, L. *Adv. Mater.* **2006**, *18*, 432–436.
(9) Neinhuis, C.; Barthlott, W. *Ann. Bot.-London* **1997**, *79*, 667–677.
(10) Park, C. I.; Jeong, H. E.; Lee, S. H.; Cho, H. S.; Suh, K. Y. *J. Colloid Interface Sci.* **2009**, *336*, 298–303.
(11) Patankar, N. A. *Langmuir* **2004**, *20*, 8209–8213.
(12) Cortese, B.; D'Amone, S.; Manca, M.; Viola, I.; Cingolani, R.; Gigli, G. *Langmuir* **2008**, *24*, 2712–2718.
(13) Manca, M.; Cortese, B.; Viola, I.; Arico, A. S.; Cingolani, R.; Gigli, G. *Langmuir* **2008**, *24*, 1833–1843.
(14) Furstner, R.; Barthlott, W.; Neinhuis, C.; Walzel, P. *Langmuir* **2005**, *21*, 956–961.
(15) Cao, L. L.; Hu, H. H.; Gao, D. *Langmuir* **2007**, *23*, 4310–4314.
(16) Choi, S. J.; Suh, K. Y.; Lee, H. H. *Nanotechnology* **2008**, *19*, 275305.
(17) Jeong, H. E.; Lee, S. H.; Kim, J. K.; Suh, K. Y. *Langmuir* **2006**, *22*, 1640–1645.
(18) Fresnais, J.; Benyahia, L.; Poncin-Epaillard, F. *Surf. Interface Anal.* **2006**, *38*, 144–149.
(19) Kim, T. Y.; Ingmar, B.; Bewilogua, K.; Oh, K. H.; Lee, K. R. *Chem. Phys. Lett.* **2007**, *436*, 199–203.
(20) Shirtcliffe, N. J.; McHale, G.; Newton, M. I.; Chabrol, G.; Perry, C. C. *Adv. Mater.* **2004**, *16*, 1929–1932.
(21) Ming, W.; Wu, D.; van Benthem, R.; de With, G. *Nano Lett.* **2005**, *5*, 2298–2301.
(22) Ma, M. L.; Mao, Y.; Gupta, M.; Gleason, K. K.; Rutledge, G. C. *Macromolecules* **2005**, *38*, 9742–9748.
(23) Tsougeni, K.; Tserepi, A.; Boulousis, G.; Constantoudis, V.; Gogolides, E. *Jpn. J. Appl. Phys. 1* **2007**, *46*, 744–750.

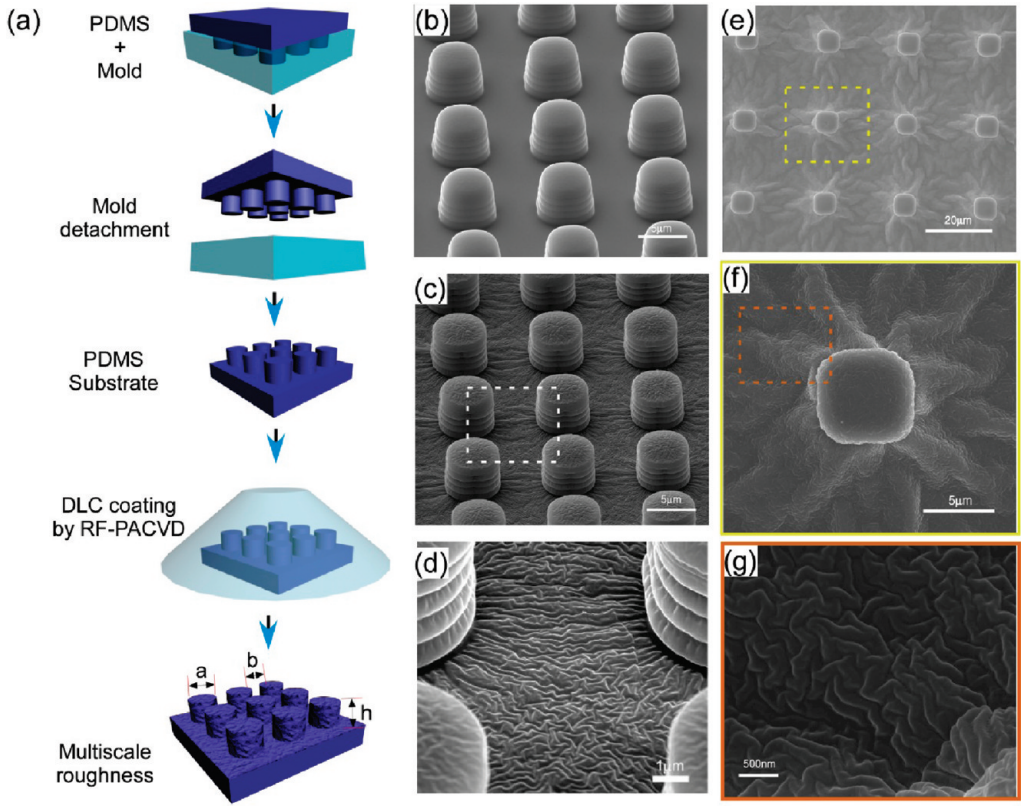

Figure 1. (a) Two-step method for the fabrication of surfaces with 3-D dual-scale surface structures, (b) PDMS surface with microscale pillar structures after step 1, (c) SEM image after deposition of DLC for 10s in step 2, (d) magnified image from Figure1c (white dotted box), (e) SEM image after deposition of DLC for 1 min in step 2, (f) magnified image of the multiscale 3-D hierarchical structure in Figure 1e (yellow-dotted box), and (g) magnified image from Figure 1f (red-dotted box).

film, which causes wrinkling due to its internal residual stress (0.54 ± 0.01 GPa) as well as large difference in Young's modulus between thin SiO_x-incorporated DLC film (72.04 ± 3.68 GPa) and PDMS substrate (~2 MPa). The high compressive stress in a DLC film originates from the knock-on implantation of carbon atoms with an optimum ion energy to overwhelm the stress relaxation during the deposition process.[24−26] Furthermore, a significant amount of sp^3 bonds would also contribute to the high compressive stress of the DLC film since the sp^3 sites tend to form a local compression stress rather than tension in the sp^2 sites.[26] In this method, typical external forces such as prestretching[27,28] and/or thermal contraction[29] of the substrate are not required to create wrinkle patterns on a compliant substrate.

In general, wrinkles can be generated in a thin hard film supported on a compliant (or soft) substrate when the film is compressed laterally and buckled.[30−32] To create such surface wrinkle patterns, several methods have been reported. For example, UV/O, oxygen, argon plasma, or ion beam has been irradiated onto the PDMS surface to make a hardened surface layer and create a compressive strain in the layer.[23,31−33] The thermally induced wrinkle formation (or buckling) is typically isotropic. To achieve anisotropic buckling, there have been various approaches using physical and (or) surface modification of the substrate prior to wrinkle formation.[28,31−33] Furthermore, a regularly ordered array of wrinkle patterns with precise shape control of individual patterns was obtained by imposing an external confinement constraint (e.g., a patterned PDMS mold) on a thin metal layer.[34]

In the current method, a one-step room-temperature coating process was employed to generate a compressively stressed, low-surface-energy DLC film with nanoscale roughness, without any external strain or subsequent annealing. A thin DLC film contains residual compressive stress in the coating layer, which can directly produce nanoscale wrinkle patterns on the prepatterned substrate as shown in Figure 1c−g. Consequently, this process results in a dual-scale surface structure of similar functionality to that of a lotus leaf. Here, hexamethyldisiloxane (HMDSO, $Si(CH_3)_3$-O-$Si(CH_3)_3$) was selected as a precursor gas for the DLC film because of its decomposition ability to form SiO_x-incorporated DLC thin film with hydrophobic nature during film deposition. In addition, the DLC coating deposited at room temperature shows long-term stability[35,36] with its superior tribological and mechanical properties as well as chemical inertness in biological

(24) Davis, C. A. *Thin Solid Films* **1993**, *226*, 30–34.
(25) Chung, J. W.; Ko, D. H.; Eun, K. Y.; Lee, K. R. *Diam. Relat. Mater.* **2002**, *11*, 1441–1446.
(26) Robertson, J. *Mat. Sci. Eng. R.* **2002**, *37*, 129–281.
(27) Groenewold, J. *Physica A* **2001**, *298*, 32–45.
(28) Chung, S.; Lee, J. H.; Moon, M. W.; Han, J.; Kamm, R. D. *Adv. Mater.* **2008**, *20*, 3011–3016.
(29) Yoo, P. J.; Lee, H. H. *Phys. Rev. Lett.* **2003**, *91*, 154502.
(30) Genzer, J.; Groenewold, J. *Soft Matter* **2006**, *2*, 310–323.
(31) Bowden, N.; Brittain, S.; Evans, A. G.; Hutchinson, J. W.; Whitesides, G. M. *Nature* **1998**, *393*, 146–149.
(32) Moon, M. W.; Lee, S. H.; Sun, J. Y.; Oh, K. H.; Vaziri, A.; Hutchinson, J. W. *Proc. Natl. Acad. Sci. U.S.A.* **2007**, *104*, 1130–1133.
(33) Efimenko, K.; Rackaitis, M.; Manias, E.; Vaziri, A.; Mahadevan, L.; Genzer, J. *Nat. Mater.* **2005**, *4*, 293–297.
(34) Yoo, P. J.; Suh, K. Y.; Park, S. Y.; Lee, H. H. *Adv. Mater.* **2002**, *14*, 1383–1387.
(35) Meskinis, S.; Gudaitis, R.; Slapikas, K.; Tamulevicius, S.; Andrulevicius, M.; Guobiene, A.; Puiso, J.; Niaura, G. *Surf. Coat. Technol.* **2008**, *202*, 2328–2331.
(36) Kopustinskas, V.; Meskinis, S.; Tamulevicius, S.; Andrulevicius, M.; Ciziute, B.; Niaura, G. *Surf. Coat. Technol.* **2006**, *200*, 6240–6244.
(37) Rahmawan, Y.; Jang, K. J.; Moon, M. W.; Lee, K. R.; Suh, K. Y. *Biochip J.* **2009**, *3*, 143–150.

environment, exhibiting biocompatibility and hemocompatibility.[37,38]

This paper is composed of two parts. First, the process of manufacturing dual-scale DLC surface structures on a PDMS substrate is described along with analysis of the formation and evolution of nanometer-scale wrinkle patterns using a simple structural buckling model. Second, wetting behaviors of a water droplet on such hydrophobic surfaces are investigated by changing the spacing ratio of the PDMS pillars and the wrinkle geometries of the coated DLC film. In characterizing the wetting behaviors, simple mathematical expressions of apparent wetting angles are derived for four different combinations of partial and total wetting angles, i.e., Cassie (C) and Wenzel (W) states, at the nano- and micrometer scales, namely, C^m-C^n, C^m-W^n, W^m-C^n, and W^m-W^n, where m and n denote micro- and nanostructures, respectively. These expressions are then used to assess the nano- and microwetting states involved in the transition behavior of the apparent wetting angle, observed experimentally when the spacing ratios of the micropillars are varied.

Experimental Section

Fabrication of Microstructures. PDMS (Sylgard 184 Silicon elastomer, Dow Corning) was used as a soft base material (Young's modulus ~2 MPa). To make pillar structures with different spacing ratios, PDMS prepolymer was cured on a silicon master prepared by photolithography. The PDMS prepolymer was cured by mixing silicon elastomer with curing agent in a ratio of 10:1 by weight. The mixture was cast on the master and baked at 70 °C for 1 h. The PDMS replica was then peeled off from the silicon master. The array of micropillars with spacing ratios from 1 to 10 was replicated from the silicon master of 4 in diameter. Each array was 1 cm × 1 cm in area, containing micropillars 4 μm in diameter and 5 μm in height.

Fabrication of Nanostructures on Microstructures. To generate nanometer-scale wrinkle structures, radio frequency plasma-assisted chemical vapor deposition (r.f. PA-CVD) was used to deposit a very thin layer of DLC onto prepatterned PDMS surfaces. The precursor gas of HMDSO was decomposed into a SiO_x-incorporated DLC film using a base pressure of 10^{-6} and a deposition pressure of 10^{-2} Torr. The r.f. bias voltage and deposition time were varied to obtain optimum surface energy and thickness of DLC coating. The typical deposition rate of DLC coating was 1.5 nm per second at r.f. bias voltage of −400 V, during which the substrate was maintained at room temperature.

Surface Characterization. Surface topography of the deposited DLC films was measured by atomic force microscopy (AFM, SIS Nanostation II) scanning on an area of 30 μm × 30 μm. The evolution of wrinkle wavelength was measured by the standard fast Fourier transform (FFT) program provided by SIS. Detailed images of hierarchical structures were taken using scanning electron microscopy (SEM, NanoSEM 200, FEI Company) with an accelerating voltage of 5 kV. A 10 nm Pt coating was used to prevent electron charging.

Contact Angle (CA) Measurements. Deionized (DI) water with a droplet volume of 5 μL was used in the measurement of static CA with sessile droplet mode. For CA measurement, advancing and receding CAs were measured when a water droplet with total volume of about 50 μL was drawn in and out onto the surfaces. The data were averaged over at least 5 different locations using a contact angle analyzer (KRUSS DSA 100).

DLC Characterization. The DLC film was deposited from an HMDSO precursor with 1 μm thickness on a bare Si [100] wafer. The mechanical properties of the DLC film were almost independent of the film thickness when deposited at optimum ion energy that is used in this work.[25] The bare Si [100] wafer (p-type boron doped), purchased from SCSA, Inc., was precleaned by sonication for 10 min in ethanol prior to wetting angle measurement and film deposition. The X-ray photoelectron spectroscopy (XPS) measurement were performed on a PHI 5800 ESCA system (Physical Electronics) using Al Kα radiation ($h\nu$ = 1486.6 eV). The residual stress of the film deposited on the Si wafer was estimated using a curvature measurement method. The hardness and Young's modulus were measured using Triboindenter TI 900, Hysitron Inc. A Berkovich diamond tip with an approximate radius of curvature of 150 nm was used as a nanoindentation tip. The load−displacement curves were recorded at 5 different points for each sample, loading continuously up to 15 mN maximum within 5 s, holding the maximum load for 5 s, and unloading completely in 5 s.

Results and Discussion

1. Fabrication and Analysis of Dual-Scale Wrinkled Pillars. In our experiments, dual-scale surface structures are made by producing nanometer-scale wrinkles on prepatterned pillar arrays of PDMS substrate. In this section, we describe the fabrication of nanowrinkled DLC thin film coating on a compliant PDMS substrate. According to previous studies,[28,31] the wrinkle wavelength, λ, of a stiff coating of thickness, t, formed under plane-strain condition is given by

$$\lambda = 2\pi t \left[\frac{(1-\nu_s^2)E_c}{3(1-\nu_c^2)E_s}\right]^{1/3} \quad (1a)$$

where E_s and E_c are Young's moduli and ν_s and ν_c Poisson's ratios with the subscripts s and c denoting the substrate and the coating, respectively. In addition, the critical compressive strain, e_c, to induce attached buckling of the film to produce wrinkles is given by[31,32]

$$e_c \approx 0.52 \left[\frac{(1-\nu_c^2)E_s}{(1-\nu_s^2)E_c}\right]^{2/3} \quad (1b)$$

and the amplitude, Ω, of wrinkle of height $h = \Omega \sin(2\pi x/\lambda)$ approaches

$$\Omega \approx \frac{\lambda}{\pi}\sqrt{e} \quad (1c)$$

for strong elastic moduli mismatch, i.e., $E_s/E_c \ll 1$, where e is the applied compressive strain ($e > e_c$). Equation 1a shows that the wrinkle wavelength elongates when the film thickness or the difference between the elastic moduli of the substrate and film increases.

Unlike other methods, deposition of a DLC film on a PDMS substrate would provide a high compressive mismatch strain in the film as well as a big difference in elastic moduli between the film and the substrate. The mechanical properties of the SiO_x-incorporated DLC film made from HMDSO are summarized in Table 1. Compared to a pure DLC film deposited from CH_4 with the same deposition technique, the SiO_x-incorporated DLC film has a lower residual stress of 0.54 ± 0.01 GPa as compared to 1.2 GPa of the pure DLC film.[39] Also, the hardness and Young's modulus were measured to be 7.86 ± 0.78 GPa and 72.04 ± 3.68 GPa, respectively, which are comparable to those of the pure DLC film of similar deposition condition reported in the literature

(38) Roy, R. K.; Lee, K. R. *J. Biomed. Mater. Res. B* **2007**, *83B*, 72–84.

(39) Cho, S. J.; Lee, K. R.; Eun, K. Y.; Jeong, J. H.; Kwon, D. *Diam. Relat. Mater.* **1999**, *8*, 1067–1072.

Table 1. Chemical Compositions and Mechanical Properties of SiO_x-Incorporated DLC Film Made from HMDSO Precursor Material along with Reference Values in the Literature

	C1s	Si2p	O1s	O/Si	C/Si	hardness (GPa)	Young's modulus, E_c (GPa)	stress (GPa)
measured value	49.40	28.45	22.15	0.78	1.74	7.86 ± 0.78	72.04 ± 3.68	0.54 ± 0.01
ref.[44]	54.4	24.3	21.3	0.9	2.1	-;	-;	-;
ref.[35]	57	23	20	0.87	2.5	-;	-;	-;

(hardness 6−10 GPa[26] and Young's modulus 50−100 GPa[39]). It is noted in this regard that the presence of the SiO_x compound in the DLC matrix is known to reduce the residual stress and increase hydrophobicity.[35,40,41]

The SiO_x-incorporated DLC film made by r.f. PA-CVD has Young's modulus of 72.04 ± 3.68 GPa as shown in Table 1 and Poisson's ratio of 0.32.[26] It is deposited on a very compliant PDMS substrate with a Young's modulus of approximately 2 MPa[42] and Poisson's ratio of 0.48.[31] These highly mismatching elastic properties determine the wavelength of the wrinkle from eq 1a as $\lambda = 136.7t$ and the critical compressive strain from eq 1b as $e_C \approx 0.05\%$. The r.f. PA-CVD setting of the film generates a mismatch compressive stress in the film equivalent to applying 0.75% lateral compressive strain on the film−substrate system as the film is deposited. This equivalent compressive strain gives rise to an amplitude of the wrinkle from eq 1c as $\Omega \approx 0.0276\ \lambda \approx 3.768t$. For example, if a film of 2 nm thickness is deposited, the wavelength of the wrinkle would be about 273 nm and the valley to peak height of the wrinkle, 2Ω, would be 15 nm. As analyzed in eqs 1a and 1b, the wavelength and the amplitude of the wrinkle can be controlled on a prepatterned PDMS substrate by varying the film thickness or the deposition time.

A schematic illustration of the fabrication procedure of the dual-scale surface roughness structures is shown in Figure 1a. Our method is based on combining both top-down and bottom-up processes. For the top-down process, direct replica molding of PDMS from a silicon master was used to produce micrometer-scale pillars 4 μm in diameter and 5 μm in height, positioned in an equally spaced square array. Specimens of ten different interpillar gap distances were made for our wetting experiments, equivalently ten different integer values of spacing ratio ranging from 1 to 10. The spacing ratio is defined as the ratio of the nearest pillar−pillar separation distance to the pillar diameter. To fabricate nanostructures on the micropillar structure surfaces, a bottom-up process was adopted by using r.f. PA-CVD of the SiO_x-incorporated DLC films from HMDSO monomer as a precursor. HMDSO was used here to form DLC films with low surface energy.[43] Upon deposition on the patterned PDMS substrate, the SiO_x-incorporated DLC film can form a wrinkle configuration in order to release the strain energy induced by its residual compression. Random orientation of a highly contorted hierarchical wrinkle structure is clearly seen after deposition of the SiO_x-incorporated DLC thin film on prepatterned pillars of PDMS; the dual-scale roughness is similar to that on a lotus leaf. Typical surface morphologies consisting of nanoscale wrinkles and microscale pillars are shown in Figure 1 for different thicknesses of DLC. In the 10 s deposition, an isotropic wrinkle pattern was formed on the top as well as on the bottom valley surfaces of the pillars as shown in Figure 1c,d. With increasing deposition time to 1 min, a dual-mode wavy structure with a primary mode of ~1.1 μm and a secondary mode of ~120 nm appeared as shown in Figure 1e−g.

Figure 2 shows the formation and evolution of the wrinkled surface with two wavy modes as a function of film thickness. According to eq 1, the wavelength of a single wavy mode would proportionally increase with the DLC film thickness, which is in agreement with our experimental data below a critical thickness of < 25 nm as shown in Figure 2a. At larger film thicknesses, the wavelength deviates from theory presumably due to coarsening of the neighboring waves. Close examination shows two wavy modes with different wavelengths: the primary (large) wavy pattern grows linearly with DLC thickness, while the secondary (small) wavy pattern shows a retarded growth on top of the primary mode wrinkle, forming a hierarchical wrinkle pattern as shown in Figure 2b. The FFT images in the inset clearly show the formation of the primary wave at small film thickness and absence of this primary wave at large film thickness by coarsening. On the basis of the results above, an optimum deposition condition for superhydrophobicity is as follows: deposition time of 30 s and base and deposition pressures of 0.01 and 10 mTorr, respectively, at a bias voltage (V) of −400 V. This process condition makes the microscale PDMS pillars covered with a uniform nanoscale DLC coating, forming a distinct dual-scale hierarchical structure.

2. Chemical Composition and Wetting Behaviors on Dual-Scale Wrinkled Pillars. Superhydrophobic effects are found in many plant leaves, animal furs, and insect wings. They can be mimicked by combining a low-surface-energy coating with micro- and nanometer scale hierarchical structures. In the current approach, superhydrophobicity is achieved by using microscale pillars covered with a nanometer-scale wrinkle pattern of SiO_x-incorporated DLC film. The DLC coating provides compressive stress for the formation of wrinkle patterns as well as a low surface energy from the HMDSO precursor material. The chemical composition of DLC film made with HMDSO is shown in Table 1 together with reference values on the basis of XPS measurements. The initial precursor stoichiometry of C/Si = 3 and O/Si = 0.5 for HMDSO is changed to C/Si = 1.74 and O/Si = 0.78 in the deposited film. The reduced stoichiometry (C/Si) of the film is due to carbon loss during deposition, while the increase of (O/Si) is probably due to surface oxidation. The XPS spectra observed here are similar to those reported by Veres et al.[44] where the main binding energy peak of C1s is accompanied by Si2p peaks of which binding energies are referred to C−Si and C−Si−O. From these results, it is clear that C−Si−O−Si−C molecular fragment of the HMDSO precursor gas is the main building block of the deposited DLC film. Namely, the C−Si−O−Si−C building block is distributed in the DLC matrix by forming direct bonding with carbon. Therefore, the characteristic of SiO_x is critical for hydrophobicity of the deposited DLC film. The building block of C−Si−O−Si−C in the SiO_x-incorporated DLC film cannot form double bonds (π-bond) and would force carbon to form sp^3 bonding while reducing the sp^2 bonding clusters. The number of bonding polarity in the film is therefore suppressed by this bonding structure, resulting in the hydrophobic nature of the DLC film.[40,43]

(40) Meskinis, S.; Tamulevicius, S.; Kopustinskas, V.; Andrulevicius, A.; Guobiene, A.; Guldaitis, R.; Liutviniene, I. *Thin Solid Films* **2007**, *515*, 7615–7618.
(41) Chen, L. Y.; Hong, F. C. N. *Diam. Relat. Mater.* **2001**, *10*, 1058–1062.
(42) Wilder, E. A.; Guo, S.; Lin-Gibson, S.; Fasolka, M. J.; Stafford, C. M. *Macromolecules* **2006**, *39*, 5956–5956.
(43) Grischke, M.; Hieke, A.; Morgenweck, F.; Dimigen, H. *Diam. Relat. Mater.* **1998**, *7*, 454–458.

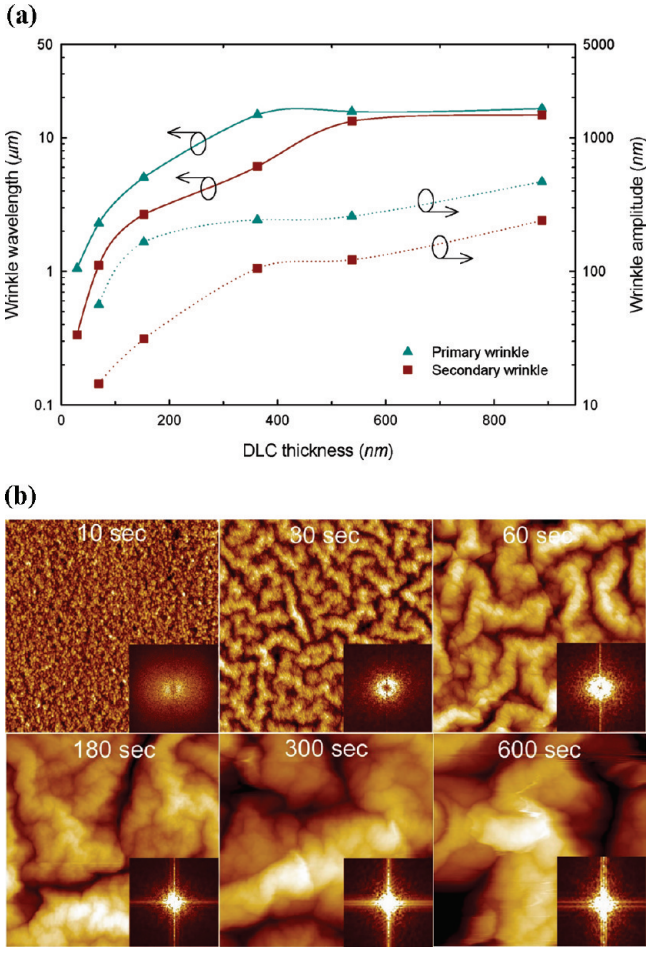

Figure 2. (a) Effect of DLC thickness on wavelength and amplitude of hierarchical wrinkle patterns with primary (long) and secondary (short) wavelengths. (b) AFM images of wrinkle morphology on PDMS substrate with FFT images in the inset.

In order to examine the effect of nanoscale roughness, we first measured wettability on two sets of substrates with initially flat surfaces; a flat Si [100] wafer and PDMS. Figure 3 shows the measurement of static CAs and roughness profiles of a thin DLC coating on both substrates. On a bare Si [100] wafer, the static CA was only 30.5°, which then increased to 106.4° after deposition of the SiO_x-incorporated DLC coating at a bias voltage of −100 V for 30 s. By increasing the magnitude of the bias voltage up to −800 V but holding the deposition time fixed for 30 s, the static CA decreased almost linearly to 86.4° shown in Figure 3a. When a higher deposition power was applied, more carbon and oxygen atoms are lost due to the high ion energies used. Therefore, the film would be rich in silicon and the wetting angle decreases accordingly. A similar trend has also been observed by Meskinis et al.[35]

On a flat PDMS substrate, a SiO_x-incorporated DLC thin film produced surface roughness in the nanoscale, thereby increasing CA from 109.9° for the uncoated PDMS up to nearly 120° for the SiO_x-incorporated DLC coated PDMS. With increasing bias voltage of the system, the deposition rate of DLC coating would increase, so that a larger wrinkle wavelength was observed as described theoretically in eq 1. As the surface is fully covered with the SiO_x-incorporated DLC on both Si and PDMS, the intrinsic contact angle of the surfaces is determined by the nature of the

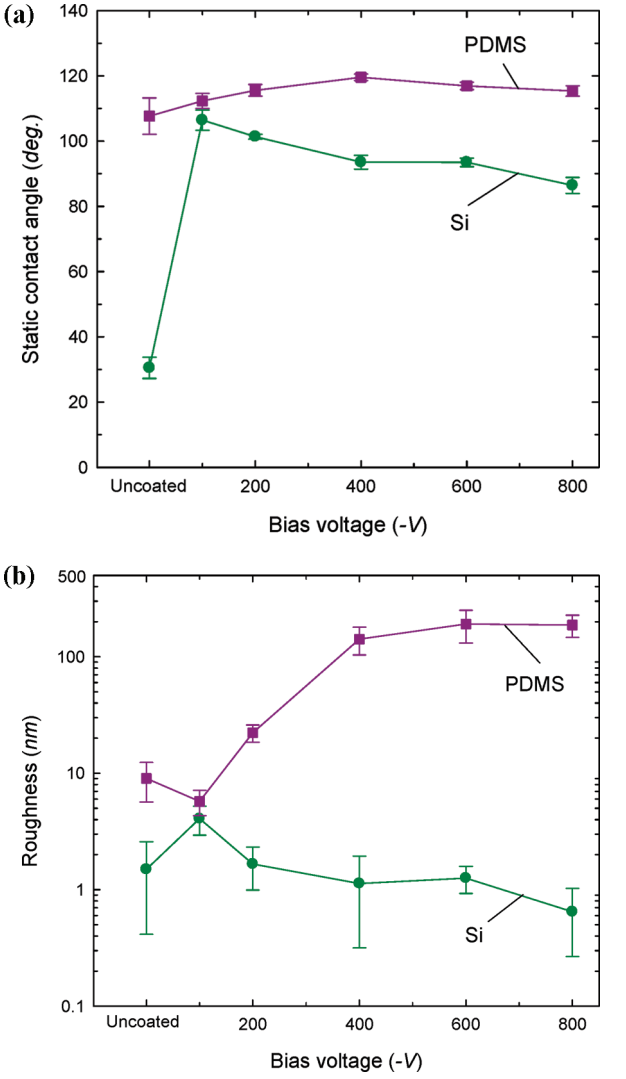

Figure 3. Hydrophobicity of DLC coatings as a function of the applied bias voltage on PDMS and Si [100] wafer. The contribution of nanoscale roughness by wrinkle patterns to the static contact angle with the respective surface chemistry changes are clearly shown in (a), while the associated surface roughness is measured in (b).

SiO_x-incorporated DLC film. Comparison of wetting angles on SiO_x-incorporated DLC coated Si and PDMS shows that the wetting angle on SiO_x-incorporated DLC/PDMS is 26° greater than that on SiO_x-incorporated DLC/Si; that difference is caused by the nanometer-scale roughness of the DLC film wrinkle on PDMS deposited at −400 V as shown in Figure 3a.

Figure 3b shows surface roughness profiles for the two sets of substrate as a function of applied bias voltage. On bare Si [100], the surface roughness decreases from 4.07 to 0.65 nm with increasing applied bias voltage, probably due to a slight increase in graphitic sp^2 hybridized bonding clusters on the SiO_x-incorporated DLC coating, producing a smoother surface. On the other hand, the surface roughness of the SiO_x-incorporated DLC coated PDMS increases from 5.7 to 191.1 nm with the applied bias voltage but plateaued at 141.6 nm after the applied bias voltage was over −400 V. The nanoscale roughness on the SiO_x-incorporated DLC coated PDMS is over 100 times higher than that on the DLC coated Si.

Next, we examine the wetting states of a water droplet on dual-scale hierarchical structures. Results demonstrate that the

(44) Veres, M.; Koos, M.; Toth, S.; Fule, M.; Pocsik, I.; Toth, A.; Mohai, M.; Bertoti, I. *Diam. Relat. Mater.* **2005**, *14*, 1051–1056.

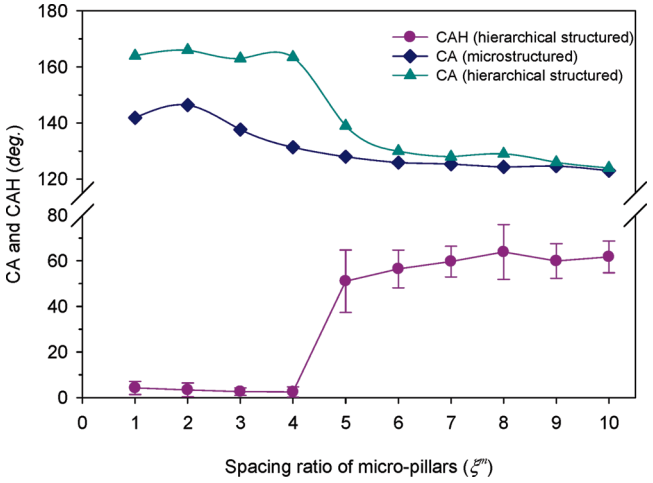

Figure 4. Static contact angle (CA) and contact angle hysteresis (CAH) of water on surfaces with microstructures and dual-scale structures.

presence of nanometer-scale wrinkles on micropillar structures significantly enhances hydrophobicity. It can be seen from Figure 4 that the static CA was maintained above 160° for the spacing ratios between 1 and 4, of the micropillars coated with a SiO_x-incorporated DLC film. At larger spacing ratios, the CA gradually decreased to 125°, which was slightly higher than that of the pure PDMS micropillar arrays. Therefore, in the presence of a SiO_x-incorporated DLC film, water droplets could not significantly wet the DLC coating—the air cushion trapped in the spacing between micropillars helped maintain a stable Cassie state. With increasing spacing, the droplet collapses and the surface loses superhydrophobicity.

In order to understand a complex wetting state on dual-roughness structures presented here, we derive mathematical models for four different wetting states, C^m-C^n, C^m-W^n, W^m-C^n, and W^m-W^n, based on energy variation analyses as shown in a schematic in Figure 5. When a water droplet is sitting on a solid surface (see Figure 5a), interface energies (or tensions) of solid/vapor (γ_S), liquid/vapor (γ_L), and liquid/solid (γ_I) are in mechanical equilibrium. Since the potential energy of the system is stationary at equilibrium, potential energy variation associated with a virtual displacement, dS_0, of the contacting line vanishes to give the expression of Young's law for an equilibrium CA, θ_e, on a molecularly flat surface as[45]

$$\cos\theta_e = \frac{(\gamma_S - \gamma_I)}{\gamma_L} \tag{2}$$

If the solid surface is rough, the apparent CA, θ^w_{app}, is affected by microscopic rough-surface wetting geometries, as proposed by Wenzel[46] and Cassie−Baxter.[47] In a Wenzel state of complete wetting, the effective interface energies (or tensions) of solid/vapor ($\bar{\gamma}_S = R\gamma_S$) and liquid/solid ($\bar{\gamma}_I = R\gamma_I$) are simply proportional to the surface roughness factor, R (= total area divided by projected area), and thus the relationship $\cos\theta^w_{app} = R\cos\theta_e$ is derived from eq 2. In a Cassie−Baxter state, a water droplet sits only on the near-top solid surfaces of the roughness with a wetting-area fraction ϕ (= partial wetting area divided by projected area), and the equilibrium condition for an apparent contact line of the microscopic wetting geometry gives $\cos\theta^C_{app} = \phi(\cos\theta_e + 1) - 1$. In both cases, the apparent CA highly depends on the microscopic geometry of the surface roughness. To take into account the effects of dual-scale roughness on CAs, we first elucidate the contact line factors (i.e., the roughness factor and the wetting-area fraction of dual-scale roughness) in the wetting analysis of the 3-D wrinkled system in the following section.

2.1. Roughness Factor and Wetting-Area Fraction of Dual-Scale Roughness. For microscale pillars used in this work, the roughness factor at the microscale is given by $R^m = 1 = \pi h/[a(1 + \xi^m)^2]$ where ξ^m is the spacing ratio, b/a, as depicted in Figure 5b. For nanoscale wrinkle structures with height variation as a one-dimensional sinusoidal waveform, $h = \Omega\sin(2\pi x/\lambda)$ as shown in Figure 5c, the nanoscale roughness factor, R^n, is simply the arc length of a period divided by the wavelength, λ, as $R^n = 1 + (\pi\Omega/\lambda)^2$. For two-dimensional wrinkles, it would be $R^n = \{1 + (\pi\Omega_1/\lambda_1)^2\}\{1 + (\pi\Omega_2/\lambda_2)^2\}$ with the subscripts 1 and 2 indicating two principal directions of the two-dimensional roughness. In Figure 5b, the microscale wetting-area fraction ϕ^m for micropillars of PDMS with a spacing ratio ξ^m is given as $\phi^m = \pi/[4(1 + \xi^m)^2]$ while the nanoscale wetting area fraction ϕ^n in Figure 5c is 0.5 based on the geometrical consideration of a sinusoidal wave.

2.2. Wetting States on Dual-Scale Surface Micro- and Nanostructures. For wetting on a surface with dual-scale surface roughness structures, there are four possible combinations of wetting states, C^m-C^n, C^m-W^n, W^m-C^n, and W^m-W^n, as described pictorially in Figure 5d−g. The theoretical CAs for each wetting state are derived as follows:

The apparent solid/vapor interface energy $\bar{\gamma}_S$ and the apparent solid/liquid interface energy $\bar{\gamma}_I$ for the four different wetting states of dual roughness, represented by [micro and nano CA state; apparent $\bar{\gamma}_S$; apparent $\bar{\gamma}_I$], can be expressed explicitly as

$$[\text{Cassie(m)} - \text{Cassie(n)}; \gamma_S\phi^n\phi^m; \gamma_I\phi^n\phi^m + \gamma_L(1 - \phi^n\phi^m)]$$

$$[\text{Wenzel(m)} - \text{Wenzel(n)}; R^mR^n\gamma_S; R^mR^n\gamma_I]$$

$$[\text{Cassie(m)} - \text{Wenzel(n)}; \gamma_S\phi^mR^n; \gamma_I\phi^mR^n + \gamma_L(1 - \phi^m)]$$

$$[\text{Wenzel(m)} - \text{Cassie(n)}; \gamma_SR^m\phi^n; \gamma_IR^m\phi^n + \gamma_L(R^m + R^m\phi^n)]$$

When we apply these apparent interface energies to the Young equation of wetting, $\cos\theta_{app} = (\bar{\gamma}_S - \bar{\gamma}_I)/\gamma_L$, we can obtain the expressions of the wetting angles for the four different states as

$$\cos\theta^{C-C}_{app} = \phi^n\phi^m(\cos\theta_e + 1) - 1 \tag{3a}$$

$$\cos\theta^{W-W}_{app} = R^mR^n\cos\theta_e \tag{3b}$$

$$\cos\theta^{C-W}_{app} = R^n\{\phi^m(\cos\theta_e + 1) - 1\} \tag{3c}$$

$$\cos\theta^{W-C}_{app} = R^m\{\phi^n(\cos\theta_e + 1) - 1\} \tag{3d}$$

Equations 3a−3d converge properly to the conventional Wenzel[46] or Cassie−Baxter[47] equation of a single scale roughness, once we substitute the wetting area fraction ϕ or the surface roughness factor R as unity for one of the two scales.

(45) Young, T. *Philos. Trans. R. Soc. London* **1805**, *95*, 65–87.
(46) Wenzel, R. N. *Ind. Eng. Chem.* **1934**, *28*, 988–994.
(47) Cassie, A. B. D.; Baxter, S. *Trans. Faraday Soc.* **1944**, *40*, 546–551.

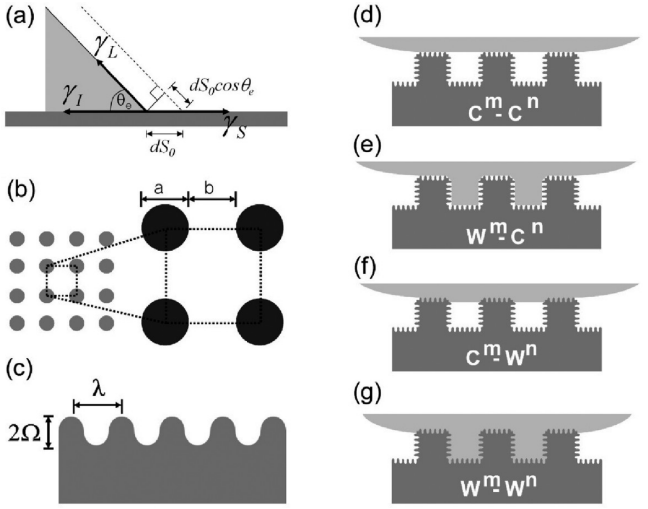

Figure 5. (a−c) Wetting profiles of water droplet on solid surfaces: (a) a schematic of contact-line variation on an idealized flat surface, (b) geometrical arrangement of micropillars (top-view), (c) a schematic geometry of nanowrinkle structures (cross-section view). (d−g) Four wetting states on dual-scale surface structures: (d) Cassie(m)-Cassie(n) state, (e) Wenzel(m)-Cassie(n) state, (f) Cassie(m)-Wenzel(n) state, (g) Wenzel(m)-Wenzel(n) state.

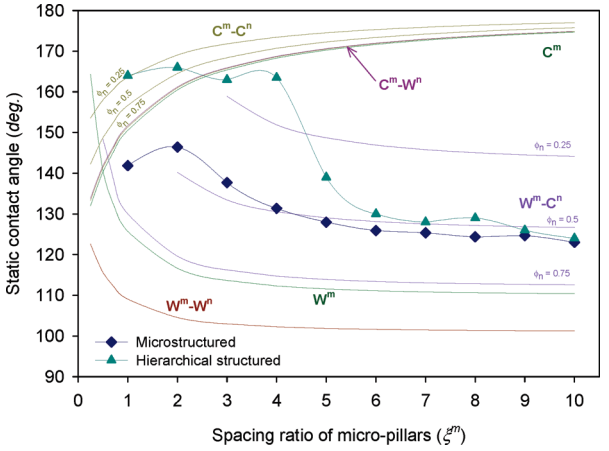

Figure 6. Comparison of wetting angles between theory and experimental data.

The theoretical CAs calculated from the above equations are plotted in Figure 6 along with the experimental data. In these plots, we first determine the nanoscale wetting area fraction by varying ϕ^n from 0.25 to 0.75 to compare with the experimental results. The multiple wetting angle measurements at high spacing ratios of micropillars covered with nanoscale wrinkle structures show that $\phi^n = 0.5$ best describes the experimental data as compared to other fractions like $\phi^n = 0.25$ or $\phi^n = 0.75$. At low spacing ratios of the micropillars, the experimental data are close to the theoretical prediction of the C^m-C^n state for all values of ϕ^n. Accordingly, it would be reasonable to take $\phi^n = 0.5$ for all the conditions used for nanoscale wrinkle structures. It is noted that our wetting model can explain wetting states of single or dual-roughness structures. For example, as ϕ^n approaches unity at low spacing ratios of micropillars, the hierarchical wetting angle prediction, C^m-C^n state approaches the single-scale Cassie state, C^m. Similarly, the hierarchical wetting angle prediction, W^m-C^n, also approaches the single-scale Wenzel state, W^m for $\phi^n = 1$. In addition, eqs 3a and 3d are reduced to single-scale Cassie and Wenzel wetting states at $\phi^n = 1$, indicating that simple mathematical models presented here can be used for general wetting analysis.

A number of notable findings are derived from the plots. For dual-scale structures with a spacing ratio of the micropillars between 1 and 2, the experimental data agree well with the theoretical predictions for the C^m-C^n state. Experimental measurements for the spacing ratios between 3 and 4 are also close to the theoretical predictions for the C^m-C^n states, but fit more closely to the predictions for the C^m-W^n states. However, it is unlikely that the CA attributes to the C^m-W^n states in this spacing-ratio range, considering our detailed experimental observations of wetting states on the nanoscale wrinkle structures. In our separate wetting experiments, the CA is measured to be approximately 120° on single-scale nanowrinkles of $R^n = 1.22$, while it is 99.6° on a flat surface. If the wetting were in a Wenzel state, the CA would have been 101.8° predicted by the Wenzel equation. On the other hand, the Cassie equation gives a CA of 125.6°, which is closer to the experimental result. In addition to the analysis of static CA, the hysteresis was very small, ranging from 2.5° to 4.2° (see Figure 4) for the spacing ratios between 1 and 4, suggesting that the wetting state is indeed C^m-C^n. Therefore, one can conclude that the Cassie state is stable on nanoscale wrinkle structures, and deviation from theory may be related to irregularities or defects on the surfaces such as scalloping (see SEM images in Figure 1) during the mold preparation process.

At spacing ratios larger than 4, the experimental results are in good agreement with the theoretical predictions for the W^m-C^n state with a high hysteresis larger than 51.1° as shown in Figure 4. As seen from Figure 6, the theoretical CAs for the W^m-W^n state are far below the experimental results, suggesting that the droplet in nanoscale wrinkle structure would be in a Cassie state regardless of the spacing ratio. In conclusion, the wetting state for 3-D dual-scale structures makes a transition from a C^m-C^n state of superhydrophobicity to a W^m-C^n state of moderate hydrophobicity as the spacing ratio increases. We believe that the stability of the Cassie state on nanoscale wrinkle structures on top of micropillar structures is essential to the formation of robust superhydrophobic surfaces.

Summary

We have presented a new method for fabricating 3-D dual-scale superhydrophobic hierarchical structures by depositing a thin coating layer of SiO_x-incorporated DLC onto PDMS micropillars. The resulting structure consists of soft PDMS micropillars covered with nanoscale DLC wrinkles. The wavelength and amplitude of these nanoscale wrinkles can be controlled by changing the thickness of the DLC coating on the prepatterned PDMS pillar array. The DLC coating provides not only a compressive stress to induce wrinkle patterns but also a low surface energy with the aid of the HMDSO precursor material.

Our experimental results show that superhydrophobicity can be achieved on the 3-D hierarchical surface structure with a low microstructure spacing ratio of 1 to 4 − the static CA was over 160° with hysteresis being as low as 3°. At larger microstructure spacing ratios, a transition to a Wenzel(m)-Cassie(n) state develops with wetting angle of approximately 130°. These findings are in line with our theoretical wetting analysis made by decoupling the wetting states on micro- and nanoroughnesses. The stable Cassie state on a low-spacing-ratio microstructure covered by low-surface-energy nanoscale wrinkle structures is the key to making robust superhydrophobic surfaces.

The simple fabrication method presented here provides an alternative method of creating 3-D hierarchically

superhydrophobic structures. These properties would be potentially useful in biomedical devices such as stents, implants, or injection syringes.

Acknowledgment. Authors are grateful to Dr. Huck-Beng Chew for helpful suggestions and comments. This work was supported by the Grant-in-Aid for Next-Generation New Technology Development Programs from the Korea Ministry of Commerce, Industry and Energy (no. 10030046), the Center for Nanoscale Mechatronics & Manufacturing (Grant 08K1401-00210), the Micro Thermal System Research Center of Seoul National University, and in part by a grant (06K1501-01610) from the CNMT under the '21st Century Frontier R&D Programs' of MEST of Korea.